Hearing Research 390 (2020) 107951

Contents lists available at ScienceDirect

Hearing Research

journal homepage: www.elsevier.com/locate/heares

Research Paper

Spatiotemporally controlled overexpression of cyclin D1 triggers generation of supernumerary cells in the postnatal mouse inner ear

Shikha Tarang [a], Umesh Pyakurel [a], Michael D. Weston [a], Sarath Vijayakumar [b, 1], Timothy Jones [b], Kay-Uwe Wagner [c, 2], Sonia M. Rocha-Sanchez [a, *]

[a] Creighton University School of Dentistry, Dept. of Oral Biology, Omaha, NE, 68178, USA
[b] University of Nebraska-Lincoln, Dept. of Special Education and Communication Disorders, Lincoln, NE, 68583-0738, USA
[c] University of Nebraska Medical Center, Eppley Institute for Research in Cancer and Allied Diseases, Omaha, NE, 68198, USA

ARTICLE INFO

Article history:
Received 14 June 2019
Received in revised form
4 February 2020
Accepted 10 March 2020
Available online 19 March 2020

Keywords:
Retinoblastoma
Cell-cycle
Cyclin D1
Supernumerary cells

ABSTRACT

The retinoblastoma family of pocket proteins (pRBs), composed of Rb1, p107, and p130 are negative regulators of cell-cycle progression. The deletion of any individual pRB in the auditory system triggers hair cells' (HCs) and supporting cells' (SCs) proliferation to different extents. Nevertheless, accessing their combined role in the inner ear through conditional or complete knockout methods is limited by the early mortality of the triple knockout. In quiescent cells, hyperphosphorylation and inactivation of the pRBs are maintained through the activity of the Cyclin-D1-cdk4/6 complex. Cyclin D1 (CycD1) is expressed in the embryonic and neonatal inner ear. In the mature organ of Corti (OC), CycD1 expression is significantly downregulated, paralleling the OC mitotic quiescence. Earlier studies showed that CycD1 overexpression leads to cell-cycle reactivation in cultures of inner ear explants. Here, we characterize a Cre-activated, Doxycycline (Dox)-controlled, conditional CycD1 overexpression model, which when bred to a tetracycline-controlled transcriptional activator and the *Atoh1-cre* mouse lines, allow for transient CycD1 overexpression and pRBs' downregulation in the inner ear in a reversible fashion. Analyses of postnatal mice's inner ears at various time points revealed the presence of supernumerary cells throughout the length of the cochlea and in the vestibular end-organs. Notably, most supernumerary cells were observed in the inner hair cells' (IHCs) region, expressed myosin VIIa (M7a), and showed no signs of apoptosis at any of the time points analyzed. Auditory and vestibular phenotypes were similar between the different genotypes and treatment groups. The fact that no significant differences were observed in auditory and vestibular function supports the notion that the supernumerary cells detected in the adult mice cochlea and macular end-organs may not impair auditory functions.

1. Introduction

The mammalian inner ear sensory epithelia, the organ of Corti (OC), consist of the sensory hair cells (HCs) and their clonally-related supporting cells (SCs). The sensory HCs, which convert mechanical stimuli into electrical signals, are organized into three rows of outer hair cells (OHCs) and one row of inner hair cells (IHCs) (Raphael and Altschuler, 2003; Dallos et al., 1996). Unlike non-mammalian vertebrates, mammals are born with a limited number of HCs, which, when lost, cannot be naturally replaced (Raphael, 2002; White et al., 2006; Cox et al., 2014; Oesterle et al., 2008). Loss of sensory HCs leads to permanent and irreversible hearing and balance deficits (Raphael, 2002).

Recent studies on HCs' and SCs' cell-cycle regulation have provided new insights into the regenerative potential in the mammalian inner ear (White et al., 2006; Schimmang and Pirvola, 2013; Rocha-Sanchez et al., 2011; Rocha-Sanchez and Beisel, 2007). Mammalian HCs' progenitor cells proliferate during embryogenesis, exit the cell-cycle, differentiate, and become functionally mature after birth (Lee et al., 2006). Post-mitotic HCs are unable to re-enter the cell-cycle and are generally referred to as 'quiescent cells' (Rocha-Sanchez and Beisel, 2007). This post-mitotic

* Corresponding author. Creighton University School of Dentistry Dept. of Oral Biology 780729 California Plaza, Omaha, NE, 68178-0731, USA.
E-mail address: ssanchez@creighton.edu (S.M. Rocha-Sanchez).
[1] Present address: Creighton University, Dept. of Biomedical Sciences, Omaha, NE, USA, 68178.
[2] Present address: Wayne State University School of Medicine, Dept. of Oncology, Barbara Ann Karmanos Cancer Institute, Detroit, MI, USA, 48201.

https://doi.org/10.1016/j.heares.2020.107951
0378-5955/

quiescence is maintained by the activity of several negative cell-cycle regulators. Consistent with that, loss of cyclin-dependent kinases (CDKs) and some of their inhibitors (e.g., $p27^{Kip1}$, p21Cip1/p19Ink4d) in the postnatal mouse OC, causes HCs and SCs to re-enter the cell cycle, proliferate, and differentiate (White et al., 2006; Chen and Segil, 1999; Laine et al., 2010a; Walters et al., 2014a; Lowenheim et al., 1999a; Minoda et al., 2007). However, as expected from permanently deleting critical regulators of the OC post-mitotic homeostasis (Rocha-Sanchez et al., 2013), these manipulations lead to apoptosis (White et al., 2006; Chen and Segil, 1999; Laine et al., 2010a; Huang et al., 2011; Weber et al., 2008a; Yu et al., 2010). Similar to the CDKs and their inhibitors, the loss of any member of the retinoblastoma (pRB) family, namely *Rb1*, p107, and p130, has been shown to stimulate cell proliferation and differentiation in the postnatal mouse OC (Rocha-Sanchez et al., 2011, 2013; Mantela et al., 2005; Sage et al., 2005, 2006). In their role as bona fide cell-cycle inhibitors, these three proteins actively interact with and repress the transcription of genes that are important for HCs and SCs proliferation and differentiation (Rocha-Sanchez et al., 2013). Interestingly, while *Rb1* deletion is followed by massive cell proliferation and apoptosis (Mantela et al., 2005; Sage et al., 2005, 2006), the deletion of either p107 or p130 results in only mild cell proliferation, without any immediate signs of apoptosis (Rocha-Sanchez et al., 2011, 2013). In all cases reported so far, the common denominator of the apoptotic death seems to be the complete and permanent inactivation of genes that are essential for the OC homeostasis.

In almost every cell in our body, cell-cycle progression is dependent on the interaction between the pRBs and Cyclin D1 (CycD1). While pRBs limit proliferation by arresting cells in the G1 to S transition of the cell-cycle, CycD1 removes the pRBs' growth inhibitory function through *G1-Cyclin D-dependent kinase*-mediated phosphorylation (Calbo et al., 2002; Nishi et al., 2009). Accordingly, pRBs are maintained in an inactive (hyper-phosphorylated) state in cells with increased *CycD1-cdk4/6* activity (Calbo et al., 2002; Nishi et al., 2009). Indeed, the nearly universal detection of mutations in components of this pathway has led to the assumption that disabling the *CycD1-Cdk4/6-Rb1* path may be required for the initiation of unscheduled proliferation in otherwise quiescent cells (Calbo et al., 2002; Nishi et al., 2009). Correspondingly, CycD1 is upregulated in the developing and neonatal OC (Laine et al., 2010b) when SCs have been shown to re-enter the cell-cycle upon stimulation with exogenous mitogens (Gu et al., 2007; Montcouquiol and Corwin, 2001; Lu and Corwin, 2008). In the mature OC, the CycD1 expression is significantly downregulated, paralleling OC permanent mitotic quiescence (Laine et al., 2010b). Moreover, CycD1 overexpression elicits cell-cycle reactivation in inner ear explants (Laine et al., 2010b). To test whether transient CycD1 overexpression in the postnatal inner ear would overcome the OC mitotic quiescence and trigger proliferation and differentiation of new HCs without inducing apoptosis, we combined the Doxycycline (Dox)-inducibility of a *CAG-βgeo-tTA-GFP* (Zhang et al., 2010) with a CycD1 overexpression model (Zhang et al., 2011a), and the *Atoh1-Cre* mouse (Matei et al., 2005) to generate an inducible *Atoh1-Cre;CAG-βgeo-tTA-GFP;TetO-CycD1-Luc (ACTTD1)*, which allow for CycD1 overexpression and, consequently, controlled and transient downregulation of all three pRBs in the mouse inner ear. Analyses of postnatal mice inner ears at various time points revealed the presence of supernumerary cells throughout the length of the cochlea and in the vestibular end-organs. Most supernumerary cells were located around the IHCs, showed signs of differentiation (e.g., the presence of apical stereocilia, expressed HC differentiation markers), and were still observed in the auditory sensory epithelia at postnatal (P) day 48, the oldest time point examined in this study. To date, there are no effective strategies and products to promote proliferation and safe regeneration of lost auditory HCs. Thus, the present study underscores a molecular pathway of potential importance for HC regeneration.

2. Materials and methods

2.1. Animals

The generation of *TetO-CycD1-IRES-Luc* and *CAG-βgeo-tTA-IRES-GFP* transgenic strains is described elsewhere (Zhang et al., 2010, 2011a). To induce CycD1 overexpression in the auditory sensory epithelia, double transgenic *CAG-βgeo-tTA-IRES-GFP/TetO-CycD1-IRES-Luc* mice were bred to *Atoh1-Cre* mice line (B6. Cg-Tg (Atoh1-cre)1Bfri/J: Jaxmice stock number 011104) to generate a triple transgenic *Atoh1-Cre-CAG-βgeo-tTA-IRES-GFP/TetO-CycD1-IRES-Luc* mouse model (Fig. 1). Pups were genotyped for: *tTA* (F - GGC TCT AGA GCC TCT GCT AAC C: R - CTT CGC TAT TAC GCC AGC TGG); *TeTO* (F - GGC GGA TGG TCT CCA CTT CGC: R - CCG TCA GAT CGC CTG GAG ACG) and *Cre* (F - GCC TGC ATT ACC GGT CGA TGC AAC GA: R - GTG GCA GAT GGC GCG GCA ACA CCA TT). Tissues from triple-positive *Atoh1-Cre*$^{+}$*-CAG-βgeo-tTA-GFP*$^{+}$*/TetO-CycD1-Luc*$^{+}$ *(ACTTD1)* transgenic mice were harvested at different postnatal (P) ages (P0, P8, P12, P18, P36, and P48). Dox administration in those animals leads to highly effective suppression of *TetO-CycD1-Luc* (Tet-Off). On the other hand, in the absence of Dox, the tTA induces very strong transactivation of the transgene (Zhang et al., 2010). Therefore, control animals consisted of mice not carrying the *Atoh1-Cre* transgene (*tTA*$^{+}$*/TetO-CycD1*$^{+}$) or triple transgenic mice (*ACTTD1*) treated with Dox. To turn-off transgene expression, the *ACTTD1* mice were treated with 2 mg/ml Dox in drinking water at P35, as described in our previous studies (Tarang et al., 2015). Unless otherwise stated for each specific method, a total of six animals per time point, genotype (e.g., *ACTTD1* and control), and technique were used in this study. All animals were treated humanely. All procedures performed were approved by the Creighton University Institutional Animal Care and Use Committee (IACUC) protocol number 0852.

2.2. Luciferase assay

Mice were intraperitoneally injected with luciferin (1 mg D-luciferin potassium salt in 0.2 ml 1 × PBS) 10 min before the imaging procedure. Inner ears were dissected out and transferred to a 96-well plate before imaging. The expression of the luciferase reporter gene associated with the *TetO-CycD1* construct was determined using *in vivo* bioluminescence imaging (IVIS200, Caliper Life Sciences, Alameda, CA).

2.3. Histological analyses

Inner ear tissues of *ACTTD1* and control animals were perfused with 4% paraformaldehyde (PFA) in phosphate-buffered saline (PBS), fixed for 72 h at 4 °C, and decalcified in 0.5M EDTA/PBS, pH 7.4 overnight. Following decalcification, the cochlear neurosensory epithelia, the organ of Corti, was dissected in PBS. The whole-mount immunohistological analysis was performed as previously described (Rocha-Sanchez et al., 2011). Briefly, OC tissue pieces (apex, middle, and base) were blocked/permeabilized in 5% NGS/0.1% Tween 20 at room temperature for 2–3h. After that, primary antibody incubations - Cyclin D1 (1:200) (Abcam #Ab16663), Myosin VIIa (M7a) (1:300) (Proteus Biosciences #25–6790), and Green Fluorescent Protein (GFP) (1:300) (Thermo Fisher #MA5-15256) were performed overnight at 4 °C. On the following day after three washes in PBS, samples were incubated in respective conjugated secondary antibodies (Life Technologies) overnight at

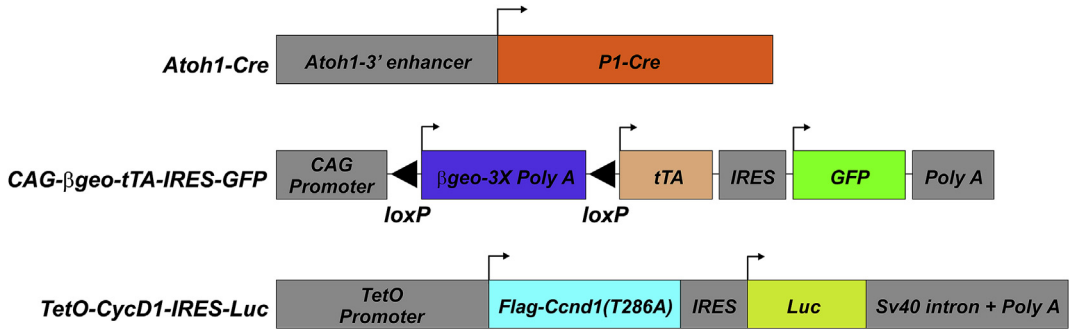

Fig. 1. The making of the *Atoh1-Cre*$^{+}$*;CAG-βgeo-tTA-IRES-GFP*$^{+}$*;TetO-CycD1-IRES-Luc*$^{+}$ *(ACTTD1)* mouse model. Breeding of the *Atoh1-Cre* (Zhang et al., 2011a) to the *CAG-βgeo-tTA-IRES-GFP* (Matei et al., 2005) mouse allow for *Cre*-mediated *loxP* recombination, removal of a transcriptional *3x poly A* (stop) sequence located between the *βgeo* promoter and the *tTA* coding sequence, and activation of the tetracycline-controlled transactivator (*tTA*, Tet-OFF) and downstream GFP reporter. Further breeding of the *Atoh1-Cre; CAG-βgeo-tTA-IRES-GFP* to the *TetO-CycD1-IRES-Luc* (Guimaraes et al., 2004) unleashes activation and overexpression of the CycD1 transgene.

4 °C. Next, samples were washed three times in PBS and mounted in prolong anti-fade mounting medium (Life Technologies) containing DAPI. Imaging was done using a Zeiss LSM 800 confocal laser microscope. Quantification of supernumerary cells was performed on 200X images obtained from three different regions (apex, middle, and base) of six *ACTTD1* and control mice cochleae. Statistical comparison between animal groups and time points was carried out using Two-Way Analysis of Variance (ANOVA) with posthoc Bonferroni correction for multiple comparisons. Values are represented as ± standard deviation (SD) of the mean. $P < 0.05$ was considered significant.

2.4. Semithin sections

Inner ear tissues of male and female *ACTTD1* and control animals were prepared as previously described (Rocha-Sanchez et al., 2011) and cut into 0.5 μm thick sections. Sections were stained with 0.1% toluidine blue (w/v in water) for 3–5sec and analyzed using a Nikon Eclipse 80i microscope.

2.5. Proliferation assay

To label mitotically active cells, a single, subcutaneous injection of the thymidine analog 5-ethynyl-2′-deoxyuridine (Edu) (50 mg/kg) in DMSO was administered to *ACTTD1* and control mice overnight before tissue harvesting. EdU incorporation into DNA of whole-mount cochleae was detected using the Click-iT EdU Alexa 488 Fluor Imaging kit (ThermoFisher Scientific #C10337) and counterstained with DAPI following the manufacturer's instructions and experimental procedures previously described (Kaiser et al., 2009). Samples were imaged using a Zeiss LSM 800 confocal laser microscope.

2.6. Real-time quantitative PCR (RT-qPCR)

Total RNA from two combined otocysts or two cochleae of WT and *ACTTD1* mice and three biological replicates at various time points was isolated using RNasy kit (Qiagen). A total of 2 μg RNA per sample was reverse transcribed as described previously (Rocha-Sanchez et al., 2011). TaqMan PCR assays (Applied Biosystems, StepOne plus system) for *CycD1* was performed in triplicate for each animal group. Relative quantitation of mRNA abundance was normalized to endogenous *β-Actin* using StepOne Software (Applied Biosystems). T-tests were performed on the normalized gene expression values to determine whether differences were statistically significant. A p-value ≤ 0.05 was considered significant.

2.7. Western blotting

ACTTD1 and control tissues (P12) were homogenized in Ripa lysis buffer (ThermoFisher Scientific #89901) with protease inhibitor (ThermoFisher Scientific #88664) using Omni Homogenizers. Lysates obtained from tissues were cleared by centrifugation at 14,000 rpm for 20 min at 4 °C. The supernatant was used for protein estimation using the Lowrey method (BioRad DC protein assay kit #500−0112). After that, 20 μg of protein was resolved on 10% SDS-PAGE and proteins were then transferred to PVDF membranes (Millipore Immobilon-P #IPVH304FO) in a Bio-Rad TransBlot apparatus per the manufacturer's instructions at 100V for 90 min. After incubation in blocking solution, the PVDF membranes were blocked in 5% blocking solution for 2h at room temperature and probed overnight using primary antibodies Cyclin D1 (Abcam #Ab16663), β-Actin (Santa Cruz # AC-15) at 4 °C. The membranes were then washed and incubated in appropriate HRP-conjugated secondary antibodies, anti-rabbit (Santa Cruz), and anti-mouse (Santa Cruz) for 1h at room temperature. After washing, peroxidase-bound protein bands were visualized by chemiluminescence using ECL substrate (Pierce, Rockford, IL, USA).

2.8. Functional assessment of auditory and vestibular function

For evoked potentials [auditory brainstem response (ABR) and vestibular sensory evoked potentials (VsEPs)] and DPOAE measures, mice were anesthetized with a ketamine (18 mg/ml) and xylazine (2 mg/ml) solution (5–9 μl per gram body weight injected intraperitoneally). Core body temperature was maintained at 37.0 ± 0.1 °C using a homeothermic heating pad system (FHC, Inc., Bowdoin, ME).

2.9. ABR stimulus and stimulus coupling

For ABR testing, tone burst stimuli were generated and controlled using Tucker Davis Technologies (TDT, Gainesville, FL) System III (RX6, PA5 components). Tone bursts at 8, 16, 32, and 41.2 kHz had 1.0 ms rise-fall times with 1.0 ms plateau (3 ms total duration) and alternating stimulus polarity. Stimuli for ABR testing were calibrated using a Bruel & Kjaar type 4138 ¼" microphone and Nexus type 2691 conditioning amplifier. Stimuli were calibrated in dB peSPL and presented via high-frequency transducers (TDT SA1 driver, MF1 speakers) coupled at the ear via PE tubing. Auditory stimuli were presented at a rate of 17 stimuli/sec.

2.10. Vestibular stimulus and stimulus coupling

VsEP recordings are based on methods for mice (Honaker et al., 2015) and are briefly described. Linear acceleration pulses, 2 ms duration, were generated and controlled with National Instruments processors and presented to the cranium via a non-invasive spring clip that encircles the head and secures it to a voltage-controlled mechanical shaker. Stimuli were presented along the naso-occipital axis using two stimulus polarities, normal (+Gx axis) and inverted (−Gx axis) at a rate of 17 pulses/sec. Stimulus amplitudes ranged from +6 dB to −18 dB re: 1.0 g/ms (where 1g = 9.8 m/s^2) adjusted in 3 dB steps.

2.11. VsEP and ABR recording

Stainless steel wire was placed subcutaneously over the skull at the nuchal crest to serve as the noninverting electrode. Needle electrodes were placed posterior to the left pinna and at the left hip for inverting and ground electrodes, respectively. Traditional signal averaging was used to resolve responses in electrophysiological recordings. The ongoing electroencephalographic activity was amplified (200,000X), filtered (300−3000Hz), and digitized (100 kHz sampling rate). 256 or 512 primary responses were averaged for each VsEP or ABR response waveform. All responses were replicated. VsEP intensity series were collected beginning at the maximum stimulus level (i.e., +6 dB re: 1.0 g/ms) with and without acoustic masking, then descending in 3 dB steps to −18 dB re: 1.0 g/ms. A broadband forward masker (50−50,000 Hz, 94 dB SPL) was presented during VsEP measurements to verify the absence of cochlear responses (Jones et al., 1999). ABR intensity series were collected with a descending series of stimulus levels (5 dB steps) beginning at approximately 110 dB peSPL.

2.12. VsEP and ABR data analysis

VsEP and ABR thresholds were defined as the stimulus level midway between the minimum stimulus level that produced a discernible response and the maximum level where no response was detectable. Thresholds were compared between knockout and wild type controls using analysis of variance (ANOVA).

2.13. DPOAE recording and data analysis

Methods for recording distortion product otoacoustic emissions (DPOAEs) were similar to those previously described (Guimaraes et al., 2004; Jimenez et al., 1999). Stimuli for DPOAEs were generated and controlled with modules from TDT. Pure tone frequencies (f1, f2, f2/f1 ratio = 1.25), at equal levels (L1 = L2 = 60 dBSPL), 150 ms duration, were generated with independent sources (TDT RX6 processor) and routed through separate drivers to mix acoustically in the ear canal (via plastic tubing placed securely at the external acoustic meatus). Stimuli were calibrated in a 0.1 ml coupler, which simulates the mouse ear canal volume. Stimulus frequencies for the primaries are such that geometric mean (GM = (f1 x f2)0.5) frequencies ranged from 6.0 to 48.5 kHz (at least eight frequencies per octave). Ear canal sound pressure levels were recorded with a low noise probe microphone (Etymotic ER 10B+). The microphone output was amplified and input to the TDT RX6 processor for digital sampling, spectral averaging, and fast Fourier transform (FFT). The amplitude of f1, f2, and the cubic difference distortion product (2f1-f2) were measured from the FFT waveform. The noise floor was measured from the amplitudes in the fifth and twelfth frequency bins above and below (±60 and 120 resp.) the 2f1-f2 component. For statistical comparison (ANOVA), the mean DPOAE amplitude across all tested primary frequency pairs was calculated and compared between knockouts and wild-type controls (Martin et al., 2007). After auditory and vestibular analyses, cochleae were processed for histological examination of supernumerary cells.

3. Results

3.1. CycD1 and transgenic constructs' expressions in the inner ear

The *ACTTD1* mouse model analyzed in this study was generated through the breeding of the three previously published lines: *Atoh1-Cre* (Matei et al., 2005), *CAG-βgeo-tTA-GFP* (Zhang et al., 2010), and the *CAG-βgeo-tTA-GFP;TetO-CycD1-Luc* (Zhang et al., 2011b) (Fig. 1). As a key regulator of the cell-cycle machinery, CycD1 is expressed during the OC development (Laine et al., 2010b). To further assess its expression in embryonic and postnatal

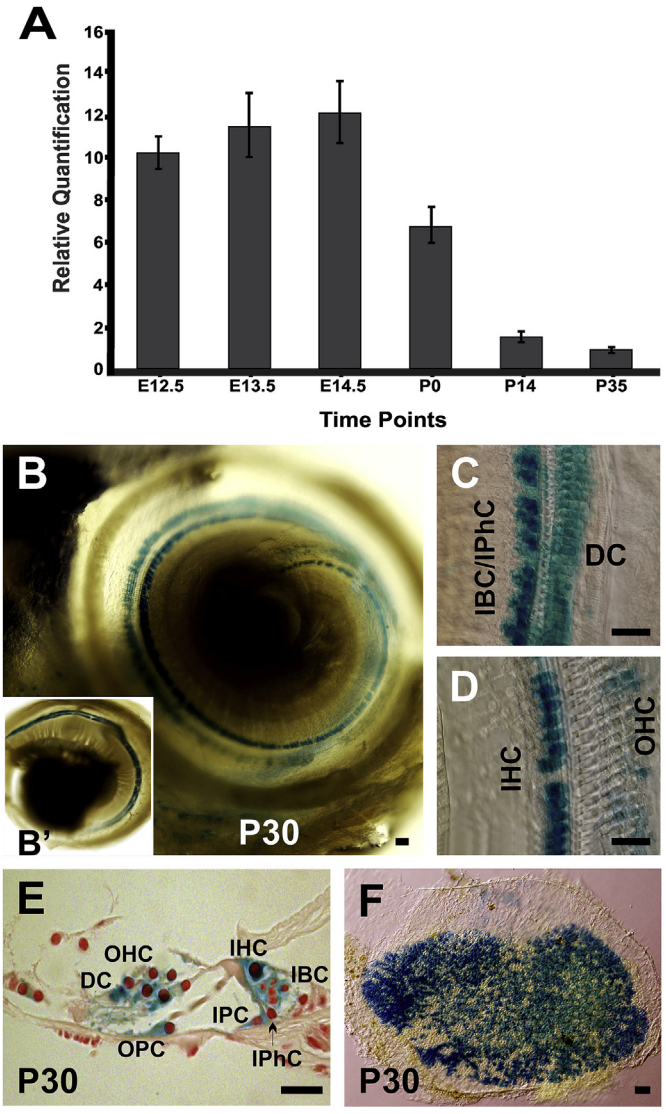

Fig. 2. CycD1 and *CAG-βgeo-tTA* expression in the WT inner ear. (**A**) Endogenous CycD1 expression in the developing and postnatal inner ear. (**B**−**F**) Specific *CAG-βgeo-tTA-GFP* expression in a P30 mouse cochlea (**B-E**) and vestibular sensory epithelia (**F**). Error bars in (A) correspond to the standard deviations of the relative expression ($2^{-(\Delta\Delta CT \pm pooled\ StDev)}$) of CycD1′ and *β-Actin's* CT values. OHC = outer hair cells; IHC = inner hair cells; DC = Deiters' cells; OPC = outer pillar cells; IPC = inner pillar cells IBC = inner border cells; IPhC = inner phalangeal cells. Bar = 10 μm.

development, we performed a temporal expression analysis of CycD1 transcripts at various embryonic (E) and postnatal (P) time points (*i.e.,* E12.5, E13.5, E14.5, P0, P14, and P35) (Fig. 2A). Consistent with its role, CycD1 levels were higher at embryonic time points (when the inner ear sensory epithelium is undergoing mitotic proliferation) and at neonatal stages (when post-mitotic sensory hair cells are still able to proliferate upon mitogenic stimulation). After that, a sharp decline in CycD1 expression was observed postnatally (Fig. 2A), when the pRBs, (particularly Rb1 and Rbl1/p130) are upregulated in the auditory sensory epithelia (Rocha-Sanchez et al., 2011). While the full-spectrum of CycD1 function in the mouse inner ear is unknown, these analyses suggest that post-mitotic quiescence in the mouse OC coincides with CycD1 downregulation.

Like CycD1, *Atoh1-Cre* expression in the auditory system has been previously established (Matei et al., 2005). Furthermore, bioluminescence imaging of mice carrying the *TetO-CycD1* transgene showed overexpression of the exogenous CycD1 in many organs of the *TetO-CycD1-Luc* (Zhang et al., 2011b). To confirm expression of the *CAG-βgeo-tTA* transgene in the auditory system, we performed β-galactosidase (β-gal) reaction on dissected *CAG-βgeo-tTA* adult mice ears (Fig. 2B–E). Confirming its expression in the auditory system, positive β-gal reaction was observed throughout the OC, particularly in Deiters' cells (DCs), inner (IPCs), and outer pillar (OPCs) cells, in IHCs and their associated SCs (Fig. 2C–E). Positive β-gal expression was also observed in OHCs; however, to a lesser degree (Fig. 2D and E). Strong β-gal reactivity was also observed in the vestibular sensory epithelia (Fig. 2F).

The *CAG-tTA*-mediated transactivation can be completely ablated through the administration of Dox while its subsequent withdrawal lifts the transcriptional block and leads to effective reactivation of *TetO*-regulated target genes (Zhang et al., 2011b). To confirm effective Dox-controlled transactivation of *CAG-tTA-GFP* and test the repressibility of *CycD1* overexpression, dissected cochleae of triple-positive P12, P26, and P48 aged *ACTTD1* mice treated or not with Dox as well as age-matched controls lacking the *Atoh1-Cre* transgene (negative controls), were submitted to bioluminescence analysis (Fig. 3A). Confirming the inducibility and prompt responsiveness of the *CAG-tTA* construct and absence of leaky *TetO-CycD1-Luc* transgene expression, positive luciferase activity was detected in non-Dox-treated *ACTTD1* mice cochleae at both P12 and P48 (Fig. 3A, lane 1, wells A, D), but not on age-matched, Dox-treated *ACTTD1* animals (Fig. 3A, lane 1, wells B, C). Negative control animals displayed no luciferase activity regardless of the absence (Fig. 3A, lane 2, wells A, D) or presence (Fig. 3A, lane 2, wells B, C) of Dox. To further assess the inducible nature of the construct and its tight Dox-dependent regulation, P21 *ACTTD1* and age-matched control mice were treated with Dox in drinking water for ten consecutive days, followed by 17 consecutive days without Dox. Contrasting with the complete lack of luciferase activity in the presence of Dox (data not shown but see Fig. 3A, lane 1, wells B, C), efficient *CAG-tTA* transgene activation was observed at P48 upon removal of Dox treatment (Fig. 3A, lane 1, well E). Once more, no changes were observed in age-matched negative control cochleae (Fig. 3A, lane 2, well E). These results were further supported by mRNA (Fig. 3B), and protein (Fig. 3C) quantification analyses, which showed CycD1 overexpression in non-Dox treated *ACTTD1* mice's inner ear.

3.2. *Atoh1-cre-mediated expression of Dox-controlled CycD1 overexpression triggers the generation of supernumerary cells in postnatal ACTTD1 mouse OC*

Given CycD1's direct effect on the regulation of the three pRBs, we pursued to understand the potential effects of its overexpression in the *ACTTD1* mouse cochleae at various postnatal time points. Whole-mount cochleae from *ACTTD1* and control animals not carrying the *Atoh1-Cre* transgene and Dox-treated *ACTTD1* animals were assessed for cell proliferation with the thymidine analog EdU (50 mg/kg) and immunohistochemistry with antibodies against the HC marker Myosin VIIa (M7a), and phalloidin (Fig. 4A–J). Additionally, to assess the efficiency of *Atoh1-Cre*-mediated recombination and activation of the *CAG-βgeo-tTA-IRES-GFP* cassette (Zhang et al., 2010), immunohistochemistry using an antibody against GFP was also performed (Fig. 4D, E and H). Of note, despite confirmed *ACTTD1* transcriptional activation in embryonic and early postnatal inner ear, a time when endogenous CycD1 is naturally upregulated (Fig. 2A) (Laine

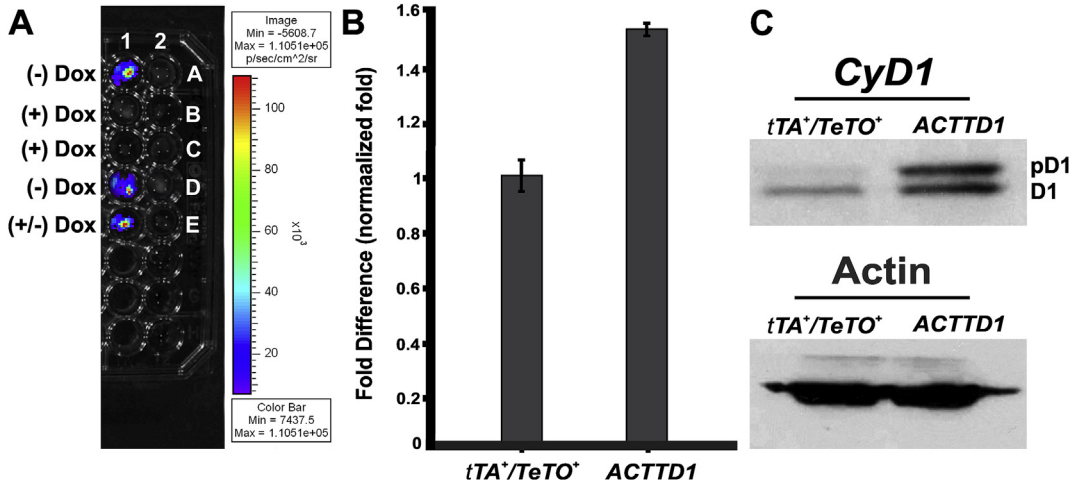

Fig. 3. *In vitro* qualitative assessment of combined the *ACTTD1* transgene responsiveness to Dox treatment. (A) Bioluminescence analysis of triple-positive *ACTTD1* mice cochleae (lane 1) and age-matched negative controls lacking *Atoh1-Cre* (lane 2) at different postnatal time points. Positive luciferase activity was detected in non-Dox-treated *ACTTD1* cochleae at P12 (lane 1, well A), and P26 (lane 1, row D), but not on age-matched, Dox-treated *ACTTD1* animals (lane 1, wells B, C, respectively). Negative control animals displayed no luciferase activity regardless of the absence (lane 2, wells A, D) or presence (lane 2, wells B, C) of Dox. Confirming the transgene's tight regulation, P48 mice, previously treated with Dox for ten days to suppress transgene activity, showed full transgene reactivation 17 days after Dox suppression (lane 1, well E). Of note, no changes were observed in the age-matched negative control cochlea lacking *Atoh1-Cre* (lane 2, well E). **(B, C)** Further supporting efficient *CAG-βgeo-tTA-GFP* transactivation, both CycD1 transcript (**B**) and protein (**C**) were upregulated in the adult *ACTTD1* OC. D1 = unphosphorylated CycD1; pD1 = phosphorylated (active) CycD1.

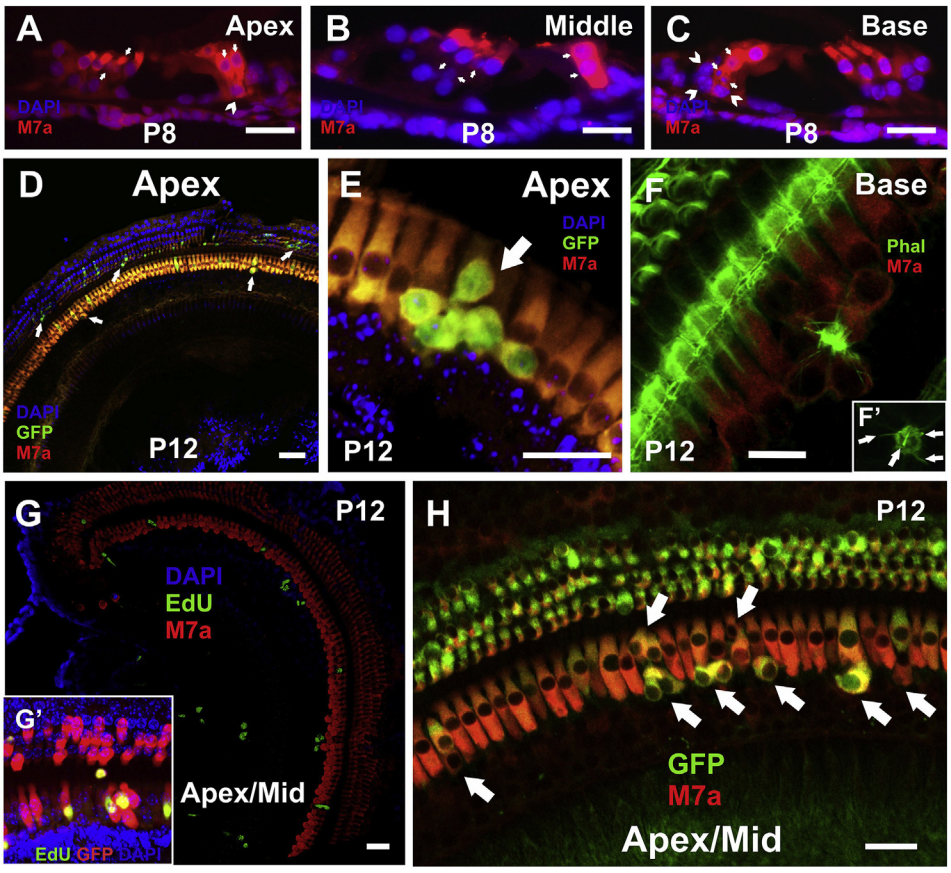

Fig. 4. Supernumerary cells in the P8 and P12 *ACTTD1* mouse cochlea. **(A–C)**. Sections of the different regions of the OC display supernumerary cells in both OHC and IHC regions. **(D).** The location of those supernumerary cells seemed to overlap with that of the GFP$^+$ (recombined) cells, which were observed in both OHC and IHC regions throughout the length of the *ACTTD1* mouse cochlea. **(E).** Supernumerary cells expressed the HC marker M7a and displayed phalloidin-positive apical projections (**F, F′**). In many instances, those clusters of supernumerary cells remained attached by their apical projections, forming flower-like structures. **(E–H)**. Consistent with a mitotic origin, EdU-positive nuclei were observed along the length of the cochleae in the proximity of the GFP$^+$ cells **(G′)**. Although GFP + cells were present in both OHCs' and IHCs' regions, most proliferation was observed around the IHCs (**G, G′**). Further supporting their origin and ability to differentiate, postmitotic, supernumerary cells co-expressed GFP and M7a (**D, E, H**). Bar = 20 μm (**A-D, G**), 10 μm (**F, H**).

et al., 2010b), no significant differences were observed in the inner ear morphology and cell numbers between *ACTTD1* and negative control mice up to one week of age (P7; data not shown). Within the second week of postnatal development, however, changes in cell numbers were already visible (Fig. 4A–C). Resembling the *βgal* (tTA) expression pattern (Fig. 2B–E) and consistent with efficient CycD1 recombination in the OC, GFP-positive (green) cells were observed throughout the length of the *ACTTD1* mouse cochlea at both OHCs and IHCs region (Fig. 4D–H). In many instances, clusters of GFP-positive supernumerary cells were found in the *ACTTD1* mouse cochleae, particularly around the IHCs (Fig. 4E). Consistent with the presence of actin-rich specialization, supernumerary cells in those clusters appeared to be attached by their phalloidin-positive apical regions (Fig. 4F, F′). Detection of EdU-positive nuclei in the same region where the supernumerary cells have been observed (Fig. 4G, G′) supports the mitotic origin of those cells. Likewise, simultaneous GFP and M7a expression in the postmitotic supernumerary cells (Fig. 4H) further corroborates their origin and ability to express an HC differentiation marker. Noteworthy, while some EdU-positive cells were observed near the OHCs, particularly at the DCs' region, most EdU-positive cells were detected around the IHCs in the inner border cells' (IBCs) and inner phalangeal cells' (IPhCs) regions (Fig. 4G, G′). Control animals displayed the standard 3:1 OHC to IHC ratio without any signs of supernumerary cells (data not shown).

3.3. Cell proliferation and survival in the postnatal ACTTD1 mouse inner ear

Previous research has demonstrated the limited, yet quantifiable, potential of neonatal mouse cochlea HCs to proliferate upon proper stimulation. However, this capacity is generally lost around 7–8 days after birth (White et al., 2006; Cox et al., 2014). To further explore the possibility of controlled CycD1 overexpression to stimulate cell proliferation in the developed inner ear, we examined the cochleae of *ACTTD1* mice at later postnatal time points. At P14, recombined (GFP$^+$) cells were abundant and observed throughout the *ACTTD1* mice cochlea (Fig. 5A-D′′). Like the younger *ACTTD1* mice, supernumerary cells were arranged in clusters scattered throughout the sensory epithelia (Fig. 5A-D′′). While some supernumerary cells were observed at the OHCs' region, most supernumerary cells were located around the IHCs, at the IBCs' and IPhCs' region (Fig. 5A–F). Although not every GFP$^+$ cell had an associated cluster of supernumerary cells, extra cells were only observed near recombined cells (Fig. 5A–D). The GFP-positive nature of the supernumerary cells, along with their distribution in the sensory epithelia, is consistent with them deriving from the IBCs' and IPhCs' cycle re-entry, rather than from the differentiated HCs (Lewis et al., 2012; Yang et al., 2010) (Fig. 5E-F). Additional lineage tracing analyses is needed to validate this preliminary observation. At P18, only a few proliferative cells were observed scattered

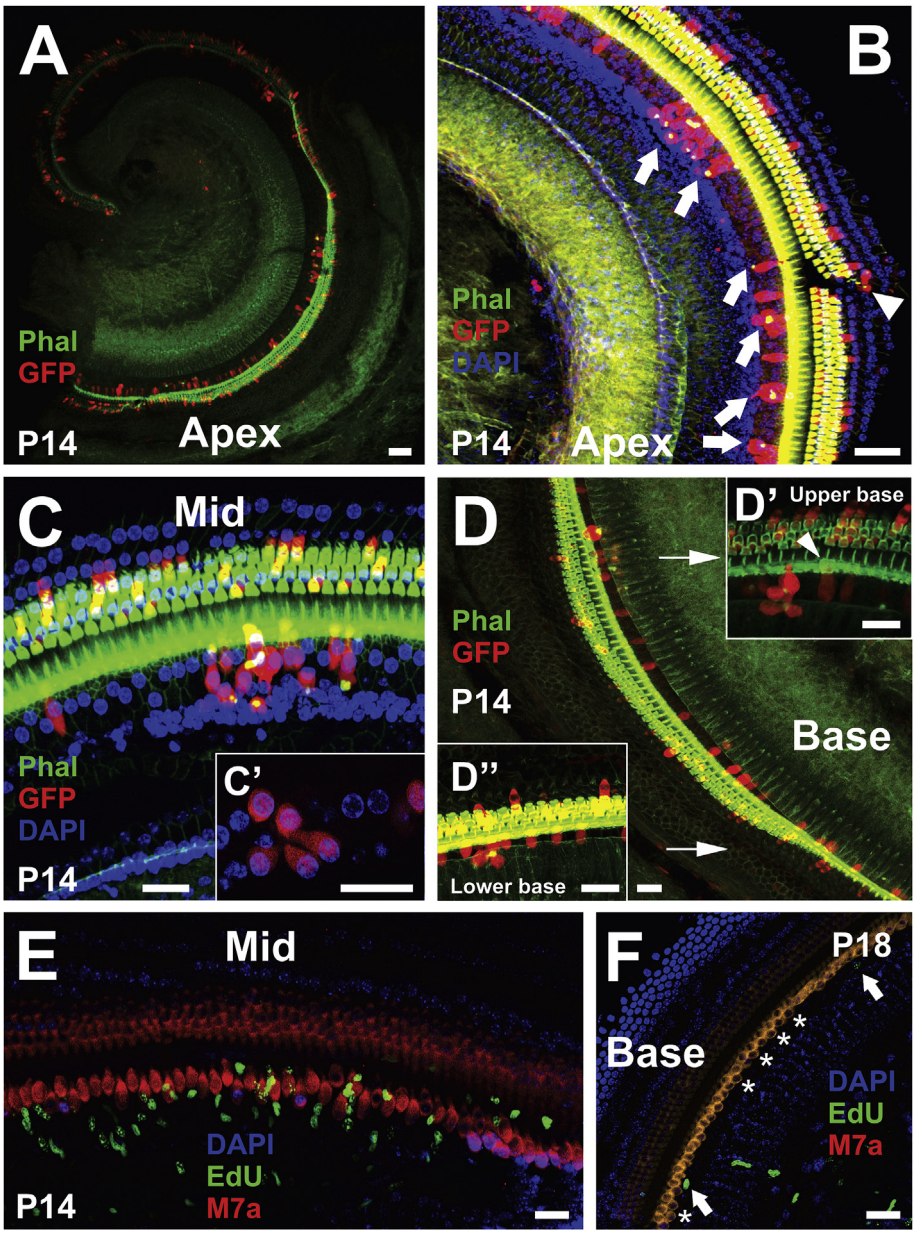

Fig. 5. Supernumerary cells in the P14, P18 *ACTTD1* mouse cochleae. **(A-D″)** Supernumerary, Edu+ supernumerary cells were still observed at P14 and P18 (**E, F**). Similar to earlier time points, the supernumerary cells were mostly arranged in a flower-like structure (**C′**), particularly noticeable near the IHCs' region (in the IPhC, and IB region). Like with earlier time points, proliferative (EdU-positive) cells were also observed at P14. By P18, the presence of proliferative cells was noticeably reduced (**F**). noteworthy, postmitotic supernumerary HCs were still observed and expressed M7a at similar levels as the regular IHCs (**F**, asterisk). Bar = 20 μm (**A, B**); 10 μm (**C**–**F**).

throughout different regions of the cochleae (Fig. 5F). By P36 and P48, no detectable signs of cell proliferation were observed, yet GFP- and M7a-positive supernumerary cells were still seen in the OC, particularly around the IHCs (Fig. 6A–G). Quantification of supernumerary cells in the ACTTD1 cochleae was performed for all four time points analyzed in this study (i.e., P8, P18, P36, and P48) (Fig. 6H). Despite age or cochlear turn (i.e., apex, middle, and base) analyzed, the average number of cells per 100 μm of cochleae was higher in ACTTD1 mice than the control group, which showed no supernumerary cells (data not shown). Within each ACTTD1 age groups, there was an overall higher concentration of supernumerary cells in the apical region ($P < 0.05$) (Fig. 6H), as compared to middle or basal turns, particularly at P8 and P36 ($P < 0.05$) (Fig. 6H). While the trend for a higher number of supernumerary cells in the apical region was still observed at P48, the difference in cell number between turns was not significant (Fig. 6H) at that time point. Comparison between P36 and P48 cochleae showed a significant decrease in supernumerary apical cells ($P < 0.05$) and an increase in cells at the basal turn ($P < 0.05$) (Fig. 6H) at the latter time point. Whether the decrease in supernumerary apical cells was due to cell death or any other factors is not yet clear. Of note, no signs of apoptosis were detected at any time point by TUNEL or Caspase-3 assays (data not shown).

Like the cochlear sensory epithelia, clusters of supernumerary cells, many of which displaying phalloidin-positive apical signals, as well as several mitotic figures, were observed in the postnatal *ACTTD1* mice vestibular end-organs' sensory epithelia (Fig. 7A–G). By P48, the latest time point analyzed, supernumerary cells were

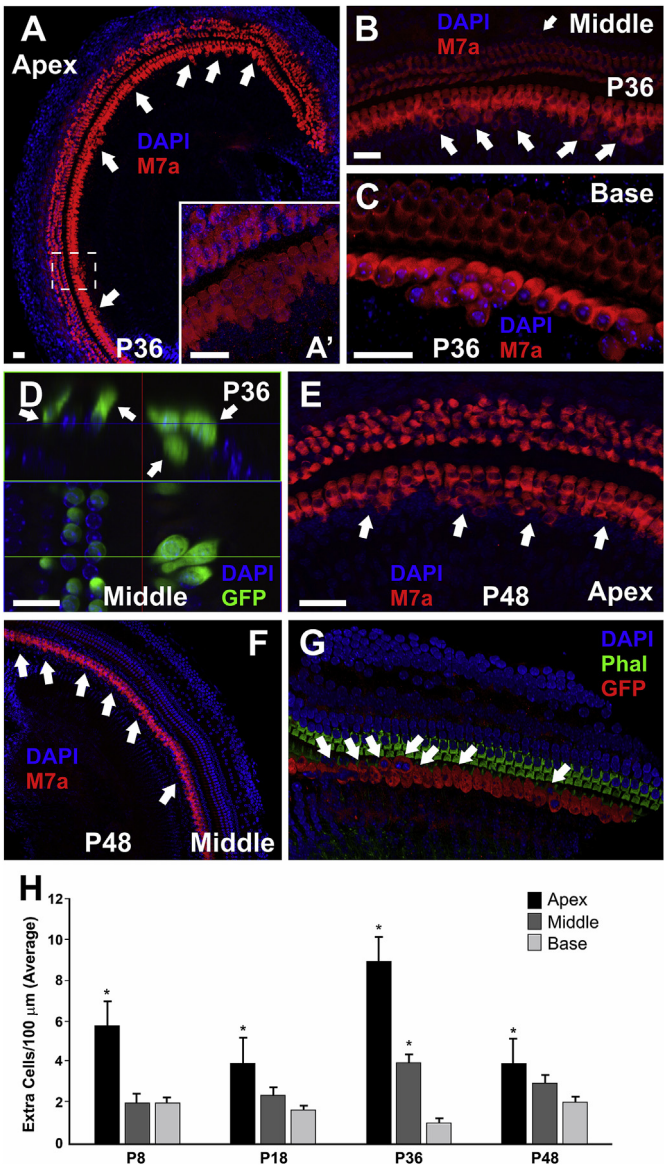

Fig. 6. Supernumerary cells in the *ACTTD1* mouse cochleae were still detected at later postnatal time points. (A–G) Although no signs of cell proliferation were observed at P36 (**A-D**) and P48 (**E-G**), supernumerary, M7a-positive cells were still observed in the apex (**A, A'**), middle (**B**), and basal (**C**) turns of the *ACTTD1* mouse cochleae. (**D**) orthogonal view from different planes (x, y, z) of an area of the confocal microscope image of the apical turn (horizontal green line) once more confirmed the location of the recombined, GFP-positive as well as supernumerary cells near the regular HCs set (arrows). (**E-G**) Except for the apical turn (**E**), where supernumerary cells still looked scattered and disorganized, most supernumerary cells in the middle (F) and basal turns of the *ACTTD1* mouse cochlea were arranged in a single row (arrows) alongside the HCs of the regular set. (**H**) Quantification of supernumerary Myosin VIIa- and GFP-positive cells in the *ACTTD1* mice cochleae at different time points revealed an overall increase in cell numbers in all three turns of the cochlea, but particularly in the apical turn independent of the animal age. The error bars represent the standard deviations for the mean apex, middle, and base HC differences between *ACTTD1* and WT mice at P8, P18, P36, and P48 from 6 different cochleae per genotype and time point. Statistical significances correspond to differences in cell numbers between the different locations in the cochleae of *ACTTD1* mice at different time points as determined by a Two-way ANOVA (Age X location) with Bonferroni's correction for multiple comparisons. *$P < 0.05$. Bar = 10 µm. (For interpretation of the references to colour in this figure legend, the reader is referred to the Web version of this article.)

still present in the vestibular sensory epithelia (Fig. 7H). No signs of mitotic proliferation were observed past P18 (Fig. 7E–G). Nevertheless, several interphasic cells displaying large nuclei, uncondensed chromatin, and large nucleoli were still observed at the vestibular supporting cells' region at P48 (Fig. 7H, arrows).

3.4. Auditory and vestibular assessment of ACTTD1 mouse model

As supernumerary cells persisted in the *ACTTD1* adult mouse inner ear, we pursued to assess the functionality of the cochleae and vestibular systems. Adult animals were divided into three different treatment groups consisting of tTA/TetO-CycD1 not carrying the *Atoh1-Cre* transgene (P33; n = 7), *ACTTD1* mice treated with Dox [*ACTTD1* (+) Dox; P45; n = 4] and the *ACTTD1* experimental group not treated with Dox [*ACTTD1* (−) Dox; P36; n = 5]. VsEPs, ABRs, and DPOAEs were completed for all groups. To confirm the presence of supernumerary cells, cochleae from all animals tested were dissected and submitted to histological analyses (Fig. 6A–H).

3.5. Vestibular function

Vestibular (VsEP) thresholds reflect the general sensitivity of the macular epithelium to the transient head motion. Mean VsEP thresholds for all treatment groups were within the normal vestibular sensitivity range (Fig. 8A). Overall, there were no significant differences in VsEPs thresholds across treatment groups (data not shown). VsEP amplitudes (p1-n1) reflect the number of primary afferent neurons contributing to the response and the degree to which they are activated synchronously with our transient stimulus. At the highest level of stimulation (+6 dB re:1 g/ms), vestibular amplitudes were within the range of amplitudes found in standard laboratory controls (Fig. 8B). Like VsEPs thresholds, there were no significant differences in VsEP amplitudes between the three treatment groups (data not shown). The encoding of the stimulus level was explored by evaluating VsEP response amplitudes as a function of stimulus level above threshold (dB SL). There were no differences in p1-n1 amplitudes between treatment groups over the three stimulus levels evidencing the largest stable sample sizes for each group (4.5, 7.5, 10.5 dB SL), thus indicating the usual response characteristics of the macular neural population for treatment groups over a wide range of stimulus levels (Fig. 8C). Vestibular latencies (p1, n1) reflect the activation timing associated with sensory transduction in hair cells and subsequent activation of the postsynaptic macular primary afferent neurons responding to our stimulus. At the highest stimulus level, latencies of both p1 and n1 were within the normal limits for laboratory control animals (Fig. 8D). There was no significant difference between groups for the first positive peak (p1). However, latencies for the experimental [*ACTTD1* (−) Dox] group were slightly shorter than the tTA/TetO-CycD1 group (mean difference 98.3 µs) but not the *ACTTD1* (+) Dox group (MANOVA, post hoc Bonf $P = 0.006$). The *ACTTD1* (+) Dox treatment group showed no differences in latency from control or *ACTTD1* (−) Dox groups. The latency difference between control and *ACTTD1* (−) Dox group disappeared when thresholds were taken into consideration and response latencies expressed in relation to each animals' threshold (dB SL, Fig. 8E). There was a normal relationship between latency and stimulus level above threshold, and there were no significant differences in latency between groups (evaluated over 4.5, 7.5, and 10.5 dB SL levels). Thus, the shorter n1 latency obtained at the highest absolute stimulus level (+6 dB re:1 g/ms) in the *ACTTD1* (−) Dox group likely reflects a slightly improved sensitivity for this group.

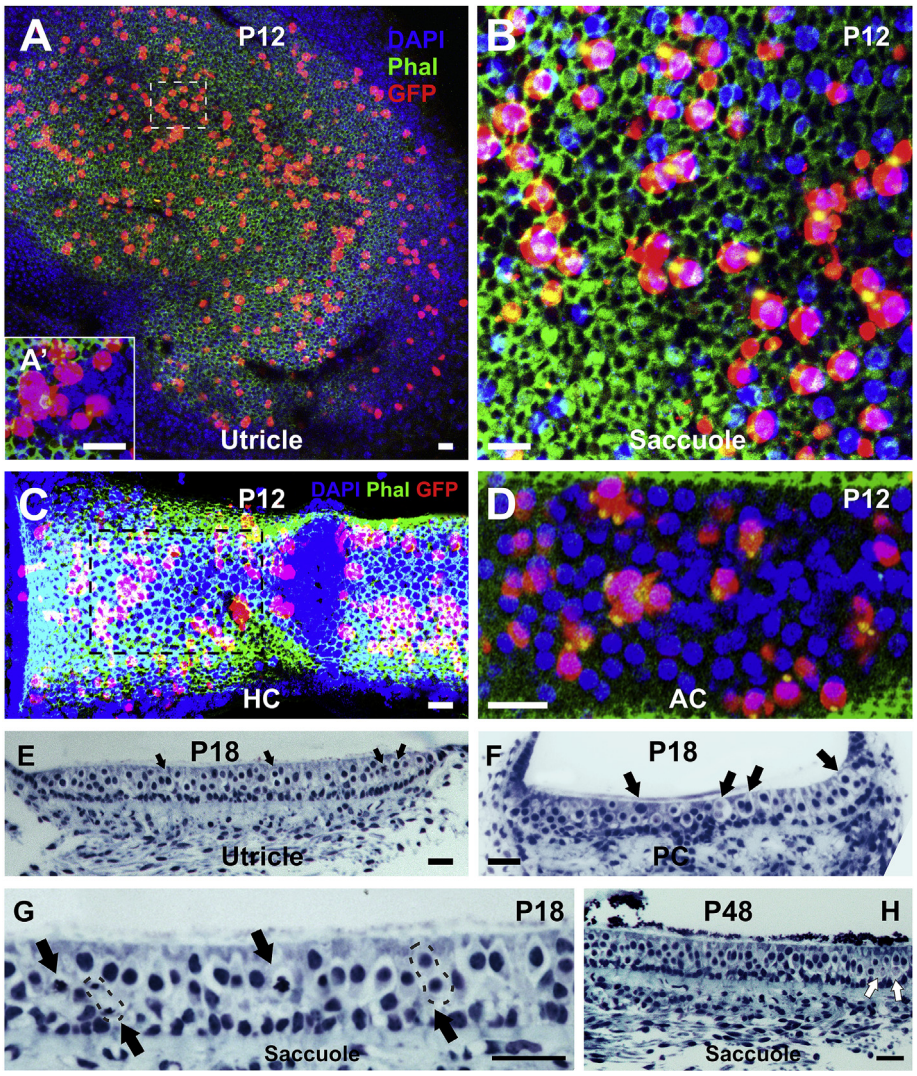

Fig. 7. Supernumerary cells in the postnatal *ACTTD1* mouse vestibular end organs **(A–D)** At P12 GFP-positive (red) and supernumerary cells were observed dispersed throughout the vestibular end-organs' sensory epithelia. Like the supernumerary cells surrounding the IHCs, the extra cells observed in the vestibular sensory epithelia were mostly arranged in clusters, forming flower-like structures (**A′, D**). (**E-F**) Further supporting their mitotic origin, toluidine blue, semi-thin (0.5 μm thick) sections of P18 *ACTTD1* mouse vestibular sensory epithelia displayed proliferating cells at different phases of the cell cycle. Dotted lines in (**G**) highlight mitotic cells. Bar = 10 μm. (For interpretation of the references to colour in this figure legend, the reader is referred to the Web version of this article.)

3.6. Auditory function

There were no significant differences in ABR thresholds at any frequency across all treatment groups (Fig. 9A–D). Likewise, the DPOAE-gram suggested relatively normal emission amplitudes from 8 to 32 KHz (Fig. 9 E). Of note, a marked reduction in emissions above 32 KHz was observed in all three treatment groups. However, based on the uniform response for all three treatment groups, it is unlikely that this reduction in emissions is due to the presence of supernumerary cells.

4. Discussion

Previous studies, ours included, have demonstrated that inactivation of any of the endogenous pRB proteins (Rb1, p107, or p130) leads to transient cell proliferation and differentiation, at varied extensions, in the mammalian inner ear (Rocha-Sanchez et al., 2011, 2013; Sage et al., 2005, 2006; Weber et al., 2008b). However, consistent with each pRB's role in the cell-cycle machinery and cellular homeostasis, newly generated HCs and SCs fail to survive (Huang et al., 2011; Yu et al., 2010; Sage et al., 2005; Weber et al., 2008b), an undesirable outcome for regenerative approaches. The possibility of collectively and transiently suppressing the combined expression of all three pRBs in the mammalian inner ear has been previously considered. However, knockout mice lacking all three pRBs are unviable (Maandag et al., 1994; Wu et al., 2003). We sought an approach at cell cycle control that extends this previous work in a novel and innovative way. We developed a system to control Cyclin D1, both spatially and temporally. Cyclin D1 is prominently implicated in the phosphorylation and inactivation of the pRBs: Underphosphorylated pRbs inhibit the cell-cycle progression while hyperphosphorylation of these proteins renders them inactive and allow the cell-cycle to progress (Rocha-Sanchez and Beisel, 2007). In this light, we sought to investigate the effects of controlled, cell-specific overexpression of CycD1 in the *ACTTD1* mouse inner ear. Under normal circumstances, endogenous CycD1 expression is postnatally downregulated in the mouse OC. However, *ACTTD1* mice displayed high levels of CycD1 expression at

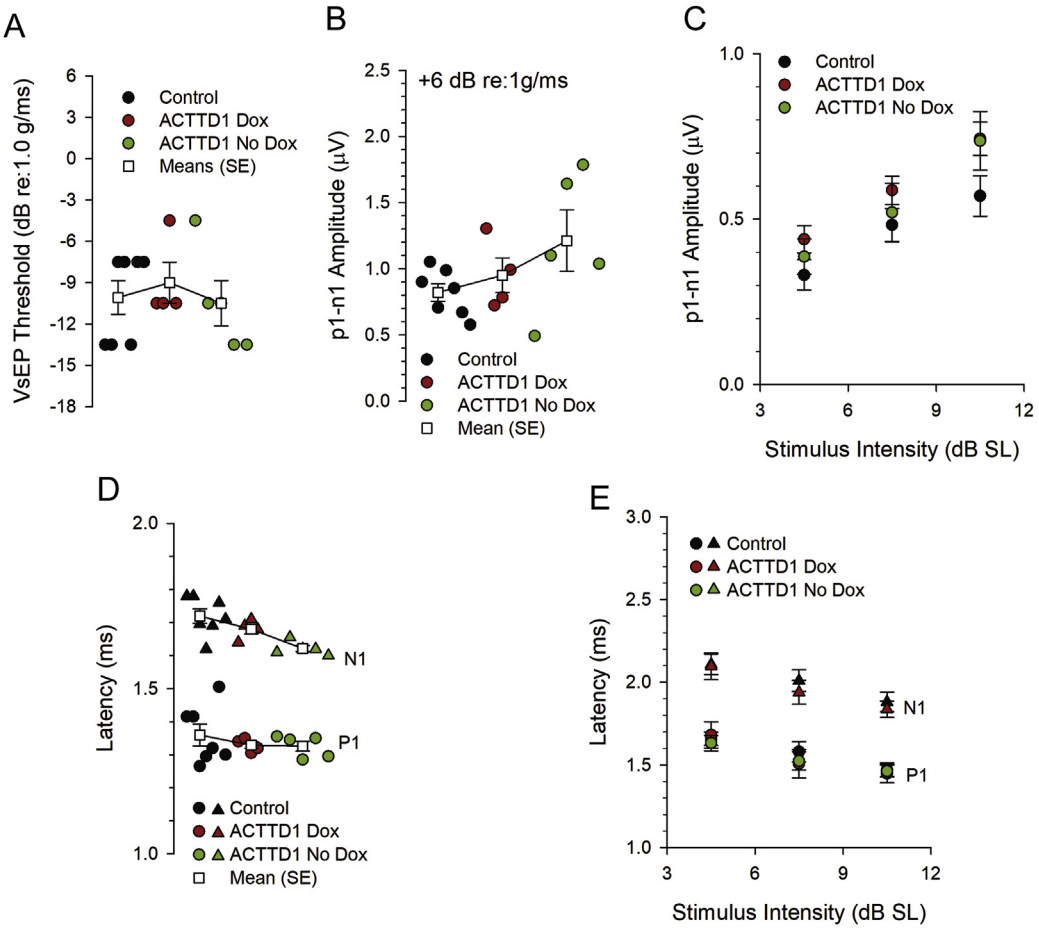

Fig. 8. Vestibular sensory-evoked potential (VsEP) responses of control and *ACTTD1* mice. (A) VsEP threshold distributions for control (black circles), *ACTTD1* mice treated with Dox (red circles) and untreated *ACTTD1* mice (green circles). Means (open squares) and SE are shown for each group. No significant differences were noted between the three groups. **(B)** At the highest stimulus level (+6 dB re: 1 g/ms), VsEP amplitude (p1-n1) was similar between the three groups. **(C)** VsEP input/output (IO) function where response amplitudes (p1−n1) are plotted as a function of stimulus level in dB SL for control, *ACTTD1* mice treated or untreated with Dox. **(D)** At the highest stimulus level (+6 dB re: 1 g/ms) VsEP latencies (p1, n1) were also similar between the three groups. **(E)** VsEP IO function where response latencies (p1, n1) are plotted as a function of stimulus level in dB SL for the three groups. All three groups showed similar VsEP response characteristics over a wide range of stimulus levels. (For interpretation of the references to colour in this figure legend, the reader is referred to the Web version of this article.)

time points when CycD1 would be naturally downregulated. Such elevated expression resulted in the presence of supernumerary cells in the postnatal inner ear. Interestingly, considering that CycD1 overexpression was controlled by a Tet-off system, no signs of unscheduled proliferation was observed before P8, when the CycD1 endogenous expression is naturally elevated in the inner ear. In a variety of different systems, the temporal regulation of protein abundance and post-translational modification is a key feature of mitotic proliferation (Ly et al., 2017; Naryzhny and Lee, 2004; Pardee, 1994). Previous studies on protein phosphorylation dynamics during the cell-cycle have also shown a normal tendency for tight regulation of protein abundance and degradation as a means to maintain a stoichiometric control of their activity (Ardito et al., 2017; Buchkovich et al., 1989; Mayol et al., 1995). As such, an increase in CycD1 synthesis when its expression is already elevated could lead to an increase in the flux of protein degradation (Alao, 2007), resulting in no changes in mitotic proliferation. Nevertheless, as the endogenous CycD1 expression went down, continued activity of the transgenic CycD1 past its normal activity time led to pRBs' hyperphosphorylation and consequential functional inactivation, as reflected by the presence of supernumerary cells in both cochleae and vestibular end-organs. Interestingly, despite the presence of recombined GFP-positive cells at both the OHCs and IHCs region in the *ACTTD1* mouse cochleae, most cell proliferation was restricted to the IHCs' region, suggesting higher plasticity of cells in that region. This observation is supported by previous studies showing differences in auditory cells' predisposition to unscheduled proliferation (Kuo et al., 2015a; Liu et al., 2012a, 2014). While lineage-tracing studies are likely to confirm the origin of those supernumerary cells, evidence collected so far (e.g., detection of GFP expression in recombined and supernumerary cells as well as the physical location of the EdU-positive and supernumerary cells) points out primarily to the IPhCs and IBCs, and DCs, to a lesser extent, as the likely source of supernumerary cells in the *ACTTD1* mouse inner ear. This observation is supported by previous report of *Atoh1-Cre* expression (Yu et al., 2010; Liu et al., 2012b), the detection of *CAG-βgeo-tTA-IRES-GFP* expression (this study), and the higher proliferative potential of SCs, particularly at the IHCs' supporting cells region. Fine-tuning of the proposed method could potentially open many avenues for the development of HC regenerative strategies. While both hair cell types are essential for hearing, the IHCs are the actual sensory receptors of the cochlea, responsible for detecting and transmitting sound information to the brain. It is estimated that 95% of the afferent auditory nerve fibers projecting to the brain arise from this subpopulation of cells (Huang et al., 2007). Although the goal is to achieve complete

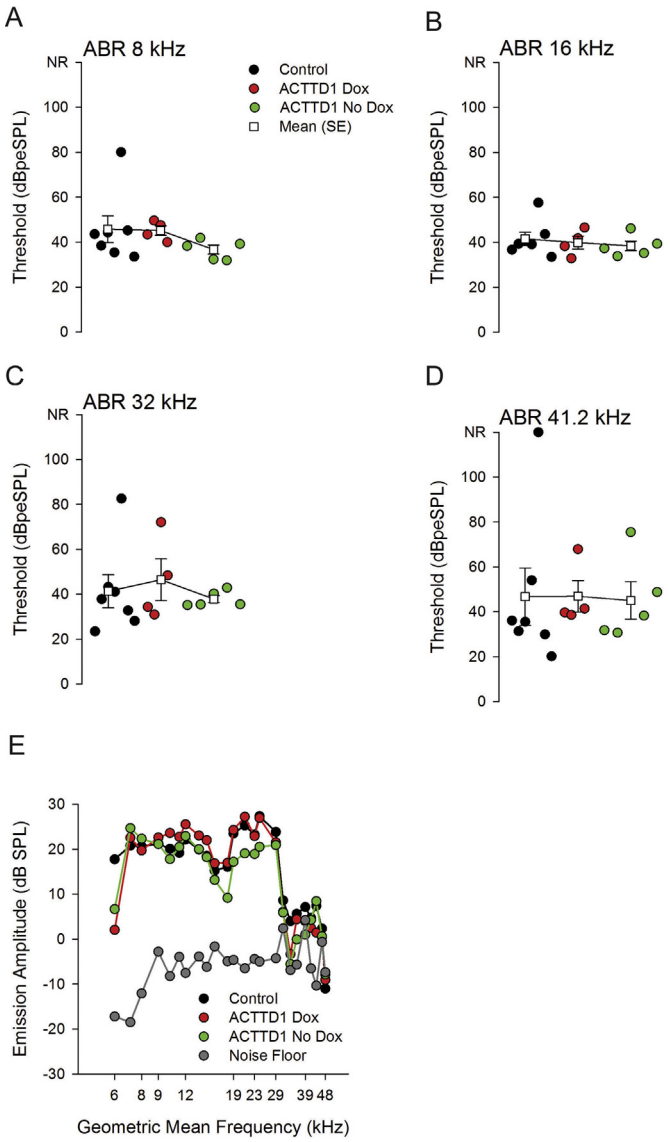

Fig. 9. Auditory function in control and *ACTTD1* mice. (A–D) Auditory brainstem response (ABR) threshold distributions in dB peSPL are represented for control and treated/untreated *ACTTD1* mice. **(E)** Distortion-product otoacoustic emission (DPOAE) amplitudes. Frequency plotted is the geometric mean of f_1 and f_2. The solid gray line represents the mean noise floor measured across all studies. Black circles – control, red circles – Dox treated *ACTTD1*, green circles – untreated *ACTTD1*. There were no significant differences in ABR thresholds of DPOAE amplitudes between the three groups. (For interpretation of the references to colour in this figure legend, the reader is referred to the Web version of this article.)

regeneration of lost auditory hair cells, successful regeneration of IHCs, particularly in older individuals, as suggested by our present findings, can have a significant impact in the field of hearing restoration and open new avenues for the pursuit of regenerative strategies.

ACTTD1 supernumerary cells are organized in characteristic 'flower-like' clusters. Moreover, most of the supernumerary cells displayed actin-rich apical specializations at all time points studied. These characteristics added to the fact that most non-dividing supernumerary cells expressed the HC marker M7a suggest that CycD1 overexpression not only unleashed unscheduled cell proliferation but most, if not all, the supernumerary cells continued to differentiate into HC-like cells. These results are supported by many others, including some of our studies, showing morphological and functional differentiation of supernumerary HCs (Laine et al., 2010b). Noteworthy, neither the presence nor the clustered organization of the supernumerary cells seems to have impacted auditory function. Like the p130 knockout mouse (Rocha-Sanchez et al., 2011), *ACTTD1* displayed near-normal hearing and vestibular function, despite the presence of supernumerary cells in both cochleae and vestibular sensory epithelia. It is important to highlight that unlike other mammalian vertebrates, human HCs are not organized in straight lines (Dallos et al., 1996; Burda and Branis, 1988). Previous reports have shown that human IHCs can be naturally arranged in small clusters without affecting auditory function (Li et al., 2018; Gubbels et al., 2008). Previous studies looking into HC regeneration through gene manipulation, p27kip knockout (Oesterle et al., 2008; Minoda et al., 2007; Liu et al., 2012b; Lowenheim et al., 1999b; Walters et al., 2014b), Atoh1-overexpression (Liu et al., 2012c, 2014; Kuo et al., 2015b; Kawamoto et al., 2003; Richardson and Atkinson, 2015; Zheng et al., 2000; Izumikawa et al., 2005), Notch signaling downregulation (Luo et al., 2017; Li et al., 2015; Mizutari et al., 2013; Pan et al., 2010), deletion of individual members of the retinoblastoma family (Rocha-Sanchez et al., 2011, 2013; Sage et al., 2005, 2006), Hes1/Hes5 modulation (Zheng et al., 2000; Abdolazimi et al., 2016; Tateya et al., 2011) among others have shown that new HCs can be generated through manipulation of different components of the HCs and SCs cell-cycle pathway. However, unlike those previous studies which involved genetic manipulation of cell-cycle genes (White et al., 2006; Cox et al., 2014), our Cyclin D1 overexpression model modulates downstream pRBs's expression post-translationally, leading to their increased hyperphosphorylation and degradation. So, while the conditional CycD1 upregulation model allows us to transiently downregulate the expression of all three pRBs in a combined fashion, it also allows for residual protein expression. This strategy allowed cells in *ACTTD1* cell-cycle re-entry at older time points (P8–P18) and remained alive for longer than previously described for other models. No evidence of cell-death was detected, as shown by negative caspase 3 staining and TUNNEL staining.

5. Conclusion

The therapeutic potential of the retinoblastoma (pRB) family (i.e., Rb1, Rbl1/p107, and Rbl2/p130) in HC regeneration has been appreciated for many years. However, no approach to date has been effective in allowing for understanding their activity in the auditory system without permanently deleting those crucial genes. The present study addresses such a lack of knowledge on the combined effect of the pRB inactivation in the auditory sensory epithelia and demonstrates that in a controlled system, postnatal auditory SCs can be stimulated to proliferate. The resultant supernumerary cells can survive for an extended period (e.g., P48) without adversely affecting auditory functions. Although preliminary, these findings add to amounting pieces of evidence already available in the literature supporting the potential of targeted and controlled manipulation of the auditory SCs' cell cycle on the development of future regenerative strategies.

Author contributions

SMR-S designed and oversaw the conduction of the experiments. ST and UP performed the experiments. ABR/DPOAE studies, data analyses, and related figures were prepared by SV and TJ. K-UW provided Cyclin D1 mice and helped with luciferase assay. ST, SMR-S wrote the manuscript. UP, MW, SV, TJ, K-UW discussed the results, helped with data analyses and did a critical revision of the article before submission. All authors have approved the final

article.

Declaration of competing interest

None.

CRediT authorship contribution statement

Shikha Tarang: Data curation, Investigation, Methodology, Writing - original draft, Writing - review & editing. **Umesh Pyakurel:** Data curation, Investigation. **Michael D. Weston:** Formal analysis, Validation, Writing - review & editing, Software. **Sarath Vijayakumar:** Data curation, Investigation, Writing - original draft. **Timothy Jones:** Data curation, Investigation, Writing - original draft. **Kay-Uwe Wagner:** Methodology, Resources, Validation. **Sonia M. Rocha-Sanchez:** Conceptualization, Formal analysis, Funding acquisition, Methodology, Project administration, Supervision, Writing - original draft, Writing - review & editing.

Acknowledgments

Technical support for luciferase imaging was provided by Drs. Kazuhito Sakamoto and Qian Zhang (UNMC). The microscopic confocal systems were made available by the UNMC Advanced Microscopy Core facility and Nebraska Center for Cell Biology (NCCB) at Creighton University. Mouse lines used in the study were maintained at Creighton University's Animal Resource Facility. This work received past support through an NIH/NCRR 5P20RR018788-NIH/NIGMS 8P20GM103471 COBRE grant (Shelley D. Smith, PI) and NIH/ORIP R21OD019745-01A1 (S.M.R.-S.).

Appendix A. Supplementary data

Supplementary data to this article can be found online at https://doi.org/10.1016/j.heares.2020.107951.

References

Abdolazimi, Y., Stojanova, Z., Segil, N., 2016. Selection of cell fate in the organ of corti involves the integration of hes/hey signaling at the Atoh1 promoter. Development 143 (5), 841–850.
Alao, J.P., 2007. The regulation of cyclin D1 degradation: roles in cancer development and the potential for therapeutic invention. Mol. Canc. 6, 24–4598, 6-24.
Ardito, F., Giuliani, M., Perrone, D., Troiano, G., Lo Muzio, L., 2017. The crucial role of protein phosphorylation in cell signaling and its use as targeted therapy (review). Int. J. Mol. Med. 40 (2), 271–280.
Buchkovich, K., Duffy, L.A., Harlow, E., 1989. The retinoblastoma protein is phosphorylated during specific phases of the cell cycle. Cell 58 (6), 1097–1105.
Burda, H., Branis, M., 1988. Postnatal development of the organ of corti in the wild house mouse, laboratory mouse, and their hybrid. Hear. Res. 36 (1), 97–105.
Calbo, J., Parreno, M., Sotillo, E., et al., 2002. G1 cyclin/cyclin-dependent kinase-coordinated phosphorylation of endogenous pocket proteins differentially regulates their interactions with E2F4 and E2F1 and gene expression. J. Biol. Chem. 277 (52), 50263–50274.
Chen, P., Segil, N., 1999. p27(Kip1) links cell proliferation to morphogenesis in the developing organ of corti. Development 126 (8), 1581–1590.
Cox, B.C., Chai, R., Lenoir, A., et al., 2014. Spontaneous hair cell regeneration in the neonatal mouse cochlea in vivo. Development 141 (4), 816–829.
Dallos, P., Popper, A.N., Fay, R.R. (Eds.), 1996. Structure of the Mammalian Cochlea, vol. 8. Springer, New York, NY. https://doi.org/10.1007/978-1-4612-0757-3_2.
Gu, R., Montcouquiol, M., Marchionni, M., Corwin, J.T., 2007. Proliferative responses to growth factors decline rapidly during postnatal maturation of mammalian hair cell epithelia. Eur. J. Neurosci. 25 (5), 1363–1372.
Gubbels, S.P., Woessner, D.W., Mitchell, J.C., Ricci, A.J., Brigande, J.V., 2008. Functional auditory hair cells produced in the mammalian cochlea by in utero gene transfer. Nature 455 (7212), 537–541.
Guimaraes, P., Zhu, X., Cannon, T., Kim, S., Frisina, R.D., 2004. Sex differences in distortion product otoacoustic emissions as a function of age in CBA mice. Hear. Res. 192 (1–2), 83–89.
Honaker, J.A., Lee, C., Criter, R.E., Jones, T.A., 2015. Test-retest reliability of the vestibular sensory-evoked potential (VsEP) in C57BL/6J mice. J. Am. Acad. Audiol. 26 (1), 59–67.
Huang, L.C., Thorne, P.R., Housley, G.D., Montgomery, J.M., 2007. Spatiotemporal definition of neurite outgrowth, refinement and retraction in the developing mouse cochlea. Development 134 (16), 2925–2933.
Huang, M., Sage, C., Tang, Y., et al., 2011. Overlapping and distinct pRb pathways in the mammalian auditory and vestibular organs. Cell Cycle 10 (2), 337–351.
Izumikawa, M., Minoda, R., Kawamoto, K., et al., 2005. Auditory hair cell replacement and hearing improvement by Atoh1 gene therapy in deaf mammals. Nat. Med. 11 (3), 271–276.
Jimenez, A.M., Stagner, B.B., Martin, G.K., Lonsbury-Martin, B.L., 1999. Age-related loss of distortion product otoacoustic emissions in four mouse strains. Hear. Res. 138 (1–2), 91–105.
Jones, S.M., Erway, L.C., Bergstrom, R.A., Schimenti, J.C., Jones, T.A., 1999. Vestibular responses to linear acceleration are absent in otoconia-deficient C57BL/6JEi-het mice. Hear. Res. 135 (1–2), 56–60.
Kaiser, C.L., Kamien, A.J., Shah, P.A., Chapman, B.J., Cotanche, D.A., 2009. 5-ethynyl-2'-deoxyuridine labeling detects proliferating cells in the regenerating avian cochlea. Laryngoscope 119 (9), 1770–1775.
Kawamoto, K., Ishimoto, S., Minoda, R., Brough, D.E., Raphael, Y., 2003. Math1 gene transfer generates new cochlear hair cells in mature Guinea pigs in vivo. J. Neurosci. 23 (11), 4395–4400.
Kuo, B.R., Baldwin, E.M., Layman, W.S., Taketo, M.M., Zuo, J., 2015. In vivo cochlear hair cell generation and survival by coactivation of beta-catenin and Atoh1. J. Neurosci. 35 (30), 10786–10798.
Kuo, B.R., Baldwin, E.M., Layman, W.S., Taketo, M.M., Zuo, J., 2015. In vivo cochlear hair cell generation and survival by coactivation of beta-catenin and Atoh1. J. Neurosci. 35 (30), 10786–10798.
Laine, H., Sulg, M., Kirjavainen, A., Pirvola, U., 2010. Cell cycle regulation in the inner ear sensory epithelia: role of cyclin D1 and cyclin-dependent kinase inhibitors. Dev. Biol. 337 (1), 134–146.
Laine, H., Sulg, M., Kirjavainen, A., Pirvola, U., 2010. Cell cycle regulation in the inner ear sensory epithelia: role of cyclin D1 and cyclin-dependent kinase inhibitors. Dev. Biol. 337 (1), 134–146.
Lee, Y.S., Liu, F., Segil, N., 2006. A morphogenetic wave of p27Kip1 transcription directs cell cycle exit during organ of corti development. Development 133 (15), 2817–2826.
Lewis, R.M., Hume, C.R., Stone, J.S., 2012. Atoh1 expression and function during auditory hair cell regeneration in post-hatch chickens. Hear. Res. 289 (1–2), 74–85.
Li, W., Wu, J., Yang, J., et al., 2015. Notch inhibition induces mitotically generated hair cells in mammalian cochleae via activating the wnt pathway. Proc. Natl. Acad. Sci. U. S. A. 112 (1), 166–171.
Li, Y., Jia, S., Liu, H., et al., 2018. Characterization of hair cell-like cells converted from supporting cells after notch inhibition in cultures of the organ of corti from neonatal gerbils. Front. Cell. Neurosci. 12, 73.
Liu, Z., Dearman, J.A., Cox, B.C., et al., 2012. Age-dependent in vivo conversion of mouse cochlear pillar and deiters' cells to immature hair cells by Atoh1 ectopic expression. J. Neurosci. 32 (19), 6600–6610.
Liu, Z., Walters, B.J., Owen, T., et al., 2012. Regulation of p27Kip1 by Sox2 maintains quiescence of inner pillar cells in the murine auditory sensory epithelium. J. Neurosci. 32 (31), 10530–10540.
Liu, Z., Dearman, J.A., Cox, B.C., et al., 2012. Age-dependent in vivo conversion of mouse cochlear pillar and deiters' cells to immature hair cells by Atoh1 ectopic expression. J. Neurosci. 32 (19), 6600–6610.
Liu, Z., Fang, J., Dearman, J., Zhang, L., Zuo, J., 2014. In vivo generation of immature inner hair cells in neonatal mouse cochleae by ectopic Atoh1 expression. PloS One 9 (2), e89377.
Lowenheim, H., Furness, D.N., Kil, J., et al., 1999. Gene disruption of p27(Kip1) allows cell proliferation in the postnatal and adult organ of corti. Proc. Natl. Acad. Sci. U. S. A. 96 (7), 4084–4088.
Lowenheim, H., Furness, D.N., Kil, J., et al., 1999. Gene disruption of p27(Kip1) allows cell proliferation in the postnatal and adult organ of corti. Proc. Natl. Acad. Sci. U. S. A. 96 (7), 4084–4088.
Lu, Z., Corwin, J.T., 2008. The influence of glycogen synthase kinase 3 in limiting cell addition in the mammalian ear. Dev. Neurobiol. 68 (8), 1059–1075.
Luo, W.W., Han, Z., Ren, D.D., Wang, X.W., Chi, F.L., Yang, J.M., 2017. Notch pathway inhibitor DAPT enhances Atoh1 activity to generate new hair cells in situ in rat cochleae. Neural Regen. Res. 12 (12), 2092–2099.
Ly, T., Whigham, A., Clarke, R., et al., 2017. Proteomic analysis of cell cycle progression in asynchronous cultures, including mitotic subphases, using PRIMMUS. eLife 6. https://doi.org/10.7554/eLife.27574.
Maandag, E.C., van der Valk, M., Vlaar, M., et al., 1994. Developmental rescue of an embryonic-lethal mutation in the retinoblastoma gene in chimeric mice. EMBO J. 13 (18), 4260–4268.
Mantela, J., Jiang, Z., Ylikoski, J., Fritzsch, B., Zacksenhaus, E., Pirvola, U., 2005. The retinoblastoma gene pathway regulates the postmitotic state of hair cells of the mouse inner ear. Development 132 (10), 2377–2388.
Martin, G.K., Vazquez, A.E., Jimenez, A.M., Stagner, B.B., Howard, M.A., Lonsbury-Martin, B.L., 2007. Comparison of distortion product otoacoustic emissions in 28 inbred strains of mice. Hear. Res. 234 (1–2), 59–72.
Matei, V., Pauley, S., Kaing, S., et al., 2005. Smaller inner ear sensory epithelia in neurog 1 null mice are related to earlier hair cell cycle exit. Dev. Dynam. 234 (3), 633–650.
Mayol, X., Garriga, J., Grana, X., 1995. Cell cycle-dependent phosphorylation of the retinoblastoma-related protein p130. Oncogene 11 (4), 801–808.
Minoda, R., Izumikawa, M., Kawamoto, K., Zhang, H., Raphael, Y., 2007. Manipulating cell cycle regulation in the mature cochlea. Hear. Res. 232 (1–2), 44–51.

Mizutari, K., Fujioka, M., Hosoya, M., et al., 2013. Notch inhibition induces cochlear hair cell regeneration and recovery of hearing after acoustic trauma. Neuron 77 (1), 58–69.
Montcouquiol, M., Corwin, J.T., 2001. Brief treatments with forskolin enhance s-phase entry in balance epithelia from the ears of rats. J. Neurosci. 21 (3), 974–982.
Naryzhny, S.N., Lee, H., 2004. The post-translational modifications of proliferating cell nuclear antigen: acetylation, not phosphorylation, plays an important role in the regulation of its function. J. Biol. Chem. 279 (19), 20194–20199.
Nishi, K., Inoue, H., Schnier, J.B., Rice, R.H., 2009. Cyclin D1 downregulation is important for permanent cell cycle exit and initiation of differentiation induced by anchorage-deprivation in human keratinocytes. J. Cell. Biochem. 106 (1), 63–72.
Oesterle, E.C., Campbell, S., Taylor, R.R., Forge, A., Hume, C.R., 2008. Sox2 and JAGGED1 expression in normal and drug-damaged adult mouse inner ear. J. Assoc. Res. Otolaryngol. 9 (1), 65–89.
Pan, W., Jin, Y., Stanger, B., Kiernan, A.E., 2010. Notch signaling is required for the generation of hair cells and supporting cells in the mammalian inner ear. Proc. Natl. Acad. Sci. U. S. A. 107 (36), 15798–15803.
Pardee, A.B., 1994. Multiple molecular levels of cell cycle regulation. J. Cell. Biochem. 54 (4), 375–378.
Raphael, Y., 2002. Cochlear pathology, sensory cell death and regeneration. Br. Med. Bull. 63, 25–38.
Raphael, Y., Altschuler, R.A., 2003. Structure and innervation of the cochlea. Brain Res. Bull. 60 (5–6), 397–422.
Richardson, R.T., Atkinson, P.J., 2015. Atoh1 gene therapy in the cochlea for hair cell regeneration. Expet Opin. Biol. Ther. 15 (3), 417–430.
Rocha-Sanchez, S.M., Beisel, K.W., 2007. Pocket proteins and cell cycle regulation in inner ear development. Int. J. Dev. Biol. 51 (6–7), 585–595.
Rocha-Sanchez, S.M., Scheetz, L.R., Contreras, M., et al., 2011. Mature mice lacking Rbl2/p130 gene have supernumerary inner ear hair cells and supporting cells. J. Neurosci. 31 (24), 8883–8893.
Rocha-Sanchez, S.M., Scheetz, L., Siddiqi, S., et al., 2013. Lack of *rbl*1/p107 effects on cell proliferation and maturation in the inner ear. J. Behav. Brain Sci. 3 (7), 534–555.
Sage, C., Huang, M., Karimi, K., et al., 2005. Proliferation of functional hair cells in vivo in the absence of the retinoblastoma protein. Science 307 (5712), 1114–1118.
Sage, C., Huang, M., Vollrath, M.A., et al., 2006. Essential role of retinoblastoma protein in mammalian hair cell development and hearing. Proc. Natl. Acad. Sci. U. S. A. 103 (19), 7345–7350.
Schimmang, T., Pirvola, U., 2013. Coupling the cell cycle to development and regeneration of the inner ear. Semin. Cell Dev. Biol. 24 (5), 507–513.
Tarang, S., Doi, S.M., Gurumurthy, C.B., Harms, D., Quadros, R., Rocha-Sanchez, S.M., 2015. Generation of a retinoblastoma (rb)1-inducible dominant-negative (DN) mouse model. Front. Cell. Neurosci. 9, 52.
Tateya, T., Imayoshi, I., Tateya, I., Ito, J., Kageyama, R., 2011. Cooperative functions of hes/hey genes in auditory hair cell and supporting cell development. Dev. Biol. 352 (2), 329–340.
Walters, B.J., Liu, Z., Crabtree, M., Coak, E., Cox, B.C., Zuo, J., 2014. Auditory hair cell-specific deletion of p27Kip1 in postnatal mice promotes cell-autonomous generation of new hair cells and normal hearing. J. Neurosci. 34 (47), 15751–15763.
Walters, B.J., Liu, Z., Crabtree, M., Coak, E., Cox, B.C., Zuo, J., 2014. Auditory hair cell-specific deletion of p27Kip1 in postnatal mice promotes cell-autonomous generation of new hair cells and normal hearing. J. Neurosci. 34 (47), 15751–15763.
Weber, T., Corbett, M.K., Chow, L.M., Valentine, M.B., Baker, S.J., Zuo, J., 2008. Rapid cell-cycle reentry and cell death after acute inactivation of the retinoblastoma gene product in postnatal cochlear hair cells. Proc. Natl. Acad. Sci. U. S. A. 105 (2), 781–785.
Weber, T., Corbett, M.K., Chow, L.M., Valentine, M.B., Baker, S.J., Zuo, J., 2008. Rapid cell-cycle reentry and cell death after acute inactivation of the retinoblastoma gene product in postnatal cochlear hair cells. Proc. Natl. Acad. Sci. U. S. A. 105 (2), 781–785.
White, P.M., Doetzlhofer, A., Lee, Y.S., Groves, A.K., Segil, N., 2006. Mammalian cochlear supporting cells can divide and trans-differentiate into hair cells. Nature 441 (7096), 984–987.
Wu, L., de Bruin, A., Saavedra, H.I., et al., 2003. Extra-embryonic function of rb is essential for embryonic development and viability. Nature 421 (6926), 942–947.
Yang, H., Xie, X., Deng, M., Chen, X., Gan, L., 2010. Generation and characterization of Atoh1-cre knock-in mouse line. Genesis 48 (6), 407–413.
Yu, Y., Weber, T., Yamashita, T., et al., 2010. Vivo proliferation of postmitotic cochlear supporting cells by acute ablation of the retinoblastoma protein in neonatal mice. J. Neurosci. 30 (17), 5927–5936.
Zhang, Q., Triplett, A.A., Harms, D.W., et al., 2010. Temporally and spatially controlled expression of transgenes in embryonic and adult tissues. Transgenic Res. 19 (3), 499–509.
Zhang, Q., Sakamoto, K., Liu, C., et al., 2011. Cyclin D3 compensates for the loss of cyclin D1 during ErbB2-induced mammary tumor initiation and progression. Canc. Res. 71 (24), 7513–7524.
Zhang, Q., Sakamoto, K., Liu, C., et al., 2011. Cyclin D3 compensates for the loss of cyclin D1 during ErbB2-induced mammary tumor initiation and progression. Canc. Res. 71 (24), 7513–7524.
Zheng, J.L., Shou, J., Guillemot, F., Kageyama, R., Gao, W.Q., 2000. Hes1 is a negative regulator of inner ear hair cell differentiation. Development 127 (21), 4551–4560.